THE JOURNAL OF PHYSICAL CHEMISTRY A

Article

pubs.acs.org/JPCA

Benzyl Radical Photodissociation Dynamics at 248 nm

Mark Shapero,[†,‡] Neil C. Cole-Filipiak,[†,‡] Courtney Haibach-Morris,[‡] and Daniel M. Neumark*[,†,‡]

[†]Chemical Sciences Division, Lawrence Berkeley National Laboratory, Berkeley, California 94720, United States

[‡]Department of Chemistry, University of California, Berkeley, California 94720, United States

ABSTRACT: The photodissociation of jet cooled benzyl radicals, C_7H_7, at 248 nm has been studied using photofragment translational spectroscopy. Two dissociation channels were observed, H + C_7H_6 and CH_3 + C_6H_4. The translational energy distribution determined for each channel suggests that both dissociation mechanisms occur via internal conversion to the ground state followed by intramolecular vibrational redistribution and dissociation. The branching ratio between these two channels has been measured to be $(CH_3 + C_6H_4)/(H + C_7H_6) = 0.011 \pm 0.004$. The dominance of the H + C_7H_6 channel is corroborated by the branching ratio calculated using Rice−Ramsperger−Kassel−Marcus theory.

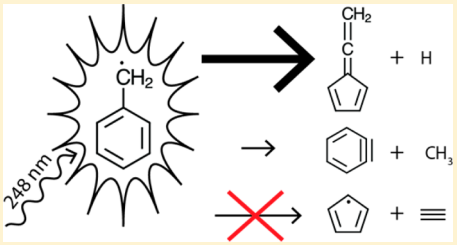

I. INTRODUCTION

The benzyl radical (C_7H_7) is ubiquitous in combustion schemes for aromatic hydrocarbons. It has been suggested as an intermediate in diesel and gasoline combustion[1] as well as a precursor to polycyclic aromatic hydrocarbons (PAHs) and soot,[2] which have negative environmental and health effects.[3] The benzyl radical is frequently encountered when modeling the combustion of toluene, for which it is the predominant decomposition product.[4−6] In addition to its bimolecular chemistry, the unimolecular decay of the benzyl radical is of interest in aromatic combustion[7,8] and is not very well understood despite the importance and small size of this species. This work aims to probe this aspect of benzyl by focusing on its photodissociation after excitation at 248 nm.

The benzyl radical was first hypothesized to exist after common spectral features were measured from related aromatic compounds in a glow discharge.[9] Since then, it has been investigated spectroscopically with numerous techniques. Its UV absorption spectrum has been measured,[10] and the electronic transition at 248 nm, first reported in 1966,[11] was assigned to the $\tilde{D}^2B_2 \leftarrow \tilde{X}^2B_2$ transition.[12] A major topic in the literature is the coupling of the first two excited electronic states of benzyl, which has been studied by fluorescence spectroscopy,[13−16] photoionization spectroscopy,[17] cavity ring down spectroscopy[18] and theoretically.[19−22] Experimental[23,24] and theoretical[1,25−29] studies of the reactions between the benzyl radical and other molecules have also been carried out.

Thermal decomposition of the benzyl radical has been extensively studied. Initial fragmentation detected with mass spectrometry following toluene pyrolysis suggested that the benzyl radical breaks apart primarily to form C_5H_5 and C_2H_2 fragments with a second dissociation channel into C_4H_4 and C_3H_3 fragments.[30] Following this initial experiment, many shock tube studies measured the decay of the benzyl radical via UV absorption and the production of H atoms by atomic resonance absorption spectroscopy (HARAS).[31] A recent review of the shock tube studies recommends a total benzyl dissociation rate constant of $(3.4 \times 10^{15})\exp(-42900/T)$ s^{-1} for the range of 1200−1750 K.[31] The recommended dissociation mechanism includes the initial suggestion of two carbon-containing fragments along with the addition of two H loss channels.[32] Subsequent shock tube studies performed with HARAS determined that H loss is the dominant dissociation channel with 0.8 H atoms produced per benzyl radical dissociated.[33,34] Deuterated shock tube studies suggested three possible benzyl decay mechanisms: H loss from the ring, H loss from the side chain, and a non-atom loss channel, required to account for the rest of the signal decay.[34]

A new technique for investigating the thermal decomposition of radicals was recently presented by Lemieux[35] and Buckingham et al.[36] A benzyl radical precursor is passed through a heated microreactor, resulting in radical formation followed by dissociation. The resulting fragments are then supersonically expanded into vacuum and detected with either photoionization mass spectrometry or matrix isolation IR spectroscopy. From these studies, many products were identified including fulvenallene (c-C_5H_4=C=CH_2), potentially the C_7H_6 fragment resulting from H loss, benzyne (c-C_6H_4), potentially from CH_3 loss, and the cyclopentadienyl radical, c-C_5H_5. However, this method cannot distinguish between primary benzyl decomposition products, secondary decomposition products, or nonunimolecular reaction products.

Limited work has been done on the photoinduced fragmentation of the benzyl radical. The fragmentation and collisional deactivation rates of vibrationally excited benzyl radicals have been measured after absorption at 308 nm.[37,38]

Special Issue: Dynamics of Molecular Collisions XXV: Fifty Years of Chemical Reaction Dynamics

Received: July 22, 2015
Revised: September 3, 2015
Published: September 8, 2015

DOI: 10.1021/acs.jpca.5b07125
J. Phys. Chem. A 2015, 119, 12349−12356

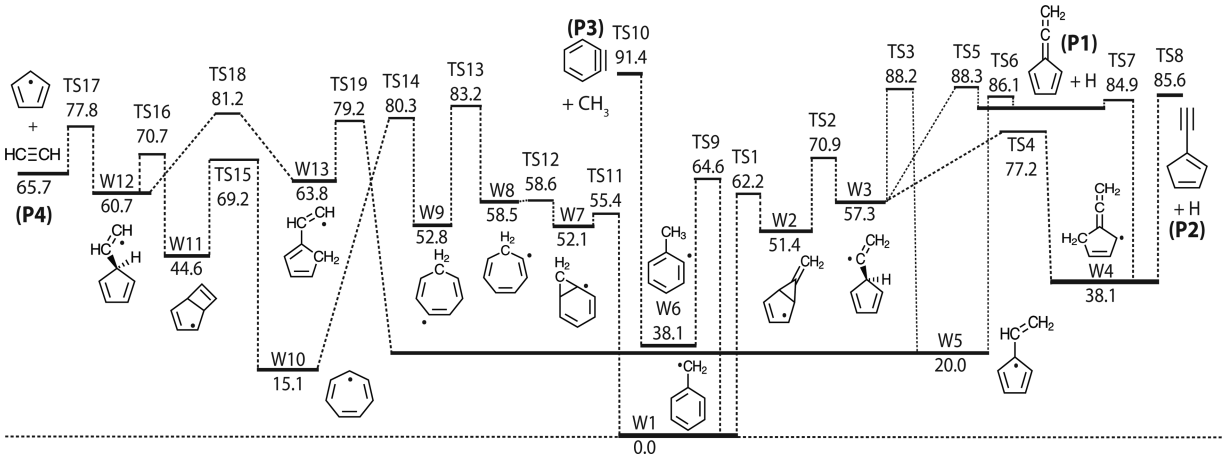

Figure 1. A simplified C_7H_7 potential energy diagram showing the production of acetylene + cyclopentadienyl, benzyne + CH_3, fulvenallene + H, and 2-ethynylcyclopentadiene + H. The energetics and pathways are compiled from refs 7, 8, 41, and 43. TS7 is shown as a well-defined transition state.[42] All energies are in kcal/mol.

Two-photon photodissociation of toluene and cycloheptatriene was studied using photofragment translational spectroscopy;[39] only an H loss channel was detected. Direct photodissociation of the benzyl radical is limited to the work by Song et al.,[40] where H atom time-of-flight spectra were measured following excitation between 228 and 270 nm. The translational energy distribution for H loss was consistent with the production of fulvenallene as the C_7H_6 product. Deuteration studies also suggested scrambling of the ring and side chain H atoms. No comment was made on any other dissociation channel, as only H atoms were measured.

Theoretical studies have proposed various benzyl dissociation mechanisms in an attempt to explain the experimental results presented above. Early theoretical mechanism predictions focused on fragmentation to two carbon-containing species,[32] but more recent studies agree that the most likely benzyl dissociation mechanism is H loss from benzyl to form fulvenallene (P1 in Figure 1).[7,8,41−43] The pathway to fulvenallene can be seen in Figure 1, which is a collection of potential energy diagrams from refs 7, 8, 41, and 43. It is initiated by benzyl cyclization to a bicyclic intermediate, W2, followed by ring opening to form a vinyl radical species, W3. From W3, there are three possible hydrogen loss pathways: (i) direct H atom dissociation from the tertiary carbon via TS5, (ii) a hydrogen transfer from the tertiary carbon to the vicinal ring carbon, W4, followed by direct H atom dissociation via TS7, and (iii) hydrogen transfer from the tertiary carbon to the CCH_2 group, W5, also followed by direct H atom dissociation via TS6. The lowest energy path, which goes through W4, is reported by Cavallotti et al.[42] to have a well-defined transition state, whereas da Silva et al.[41] employed variational transition state theory to determine the transition state.

Another C_7H_6 isomer, 2-ethynylcyclopentadiene (P2 in Figure 1), has been proposed as an alternative to the production of fulvenallene, and a recent calculation shows that it can account for as much as 20% of the C_7H_6 product.[8] Its formation proceeds as a direct H loss from the terminal carbon in W4.

To account for the deuterated experimental results,[34,40] which suggest that H loss can occur from a ring or side chain H atom, Derudi et al.[7] examined new possible decomposition mechanisms. A competitive CH_3 loss channel was found that allows for H atom scrambling between the ring and the side chain of benzyl, which was not possible in the proposed fulvenallene pathways. This CH_3 loss pathway, as shown in Figure 1, begins with a hydrogen transfer from the benzyl ring to the side chain, W6, followed by a direct dissociation of the methyl group to form benzyne (P3 in Figure 1).

The competing formation of c-C_5H_5 and C_2H_2 was also considered through a series of isomerization steps from benzyl and from a subsequent recombination of H and fulvenallene.[42,43] The mechanism for acetylene and cyclopentadienyl production from benzyl can occur through two different pathways as shown in Figure 1. In the first mechanism, the benzyl radical can isomerize to the tropyl radical, c-C_7H_7 (W1 → W7 → W8 → W9 → W10), followed by the formation of a bicyclic intermediate, W11. This intermediate can undergo ring opening to W12 and a subsequent loss of C_2H_2 to form the products, P4. The other mechanism proceeds from W5 with two consecutive hydrogen transfer reactions to W13, then W12 followed by the formation of products, P4.[43]

Higher energy pathways to other products exist, although they are not expected to play an important role in thermal benzyl decomposition.[42] From a survey of the recent theoretical work[7,8,41−43] and experimental observations,[30,34,36,40] the benzyl radical dissociation channels of interest in this work are

$$\text{benzyl} \rightarrow \text{fulvenallene} + \text{H}, \quad \Delta H_{0K} = 80.4 \text{ kcal/mol}^{42} \tag{1}$$

$$\rightarrow \text{2-ethynylcyclopentadiene} + \text{H}, \quad \Delta H_{0K} = 85.6 \text{ kcal/mol}^{8} \tag{2}$$

$$\rightarrow \text{benzyne} + \text{methyl}, \quad \Delta H_{0K} = 91.4 \text{ kcal/mol}^{7} \tag{3}$$

$$\rightarrow \text{cyclopentadienyl} + \text{acetylene}, \quad \Delta H_{0K} = 65.7 \text{ kcal/mol.}^{43} \tag{4}$$

In order to gain additional insights into the unimolecular decay of the benzyl radical, we have carried out a study of its collisionless ultraviolet photodissociation dynamics at 248 nm using molecular beam photofragment translational spectroscopy.[44] This experiment can in principle detect channels 1−4 and

DOI: 10.1021/acs.jpca.5b07125
J. Phys. Chem. A 2015, 119, 12349−12356

thus determine if processes other than H atom loss occur. We do in fact observe a small amount of CH_3 loss producing the benzyne fragment, channel 3, in addition to H loss, which is most likely from channel 1. Translational energy distributions for both channels are consistent with internal conversion to the ground electronic state followed by statistical decay. The experimental branching ratio compares well to Rice–Ramsperger–Kassel–Marcus (RRKM) calculations.

II. EXPERIMENTAL SECTION

Benzyl radical photodissociation was studied on a modified crossed molecular beam apparatus with a fixed source and rotatable detector as described previously.[45−47] A pulsed benzyl radical beam was produced by flash pyrolysis of 2-phenylethyl nitrite as it passed through a resistively heated SiC tube attached to the nozzle of a piezoelectric pulsed valve.[48,49] The resulting net reaction is shown in Scheme 1.

Scheme 1. Pyrolytic Generation of Benzyl Radicals from the Precursor 2-Phenylethyl Nitrite[49]

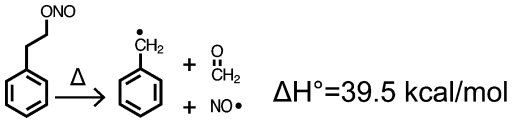

The radical precursor, 2-phenylethyl nitrite, was synthesized from 2-phenylethanol[50] and verified to be >90% pure via ^{1}H NMR (the other <10% being unreacted 2-phenylethanol). A gas mixture of 1.2 atm of ∼10% N_2 in He bubbled through an ice–water cooled sample of 2-phenylethyl nitrite was used to back the pulsed valve; in previous work,[51] this gas mixture was found to give better vibrational cooling of pyrolytically generated radicals than pure He.

The molecular beam was collimated with two skimmers that separate the source chamber from the main scattering chamber. The collimated beam was crossed at 90° with a focused, unpolarized laser pulse with a fluence of 50 mJ/cm^2 at 248 nm from a GAM EX100/500 excimer laser. The pulsed valve and laser were operated at 200 and 100 Hz, respectively, which allowed for background subtraction from the radical beam. The scattered photofragments were detected as a function of laboratory angle Θ_{Lab} in the plane defined by the laser and the molecular beam. After passing into a triply differentially pumped detector, the photofragments were ionized via electron impact ionization with 70 eV electrons. The resulting ions were mass-selected with a quadrupole mass filter and detected with a Daly style ion detector.[52] The ion signal as a function of time relative to the laser pulse was acquired with a multichannel scalar interfaced with a computer for 10^5−10^6 laser shots. These time-of-flight (TOF) spectra were simulated using a forward convolution method to iteratively determine the center-of-mass translational energy distributions for each product channel.

Mass spectra of the molecular beam were used to verify 2-phenylethyl nitrite depletion (m/z = 151) and benzyl radical formation (m/z = 91); examples are shown in Figure 2. The gray trace is the precursor mass spectrum taken with pyrolysis off; the parent peak is visible at m/z = 151. With pyrolysis on, the parent peak disappears and the resulting mass spectrum (black line, Figure 2) matches the literature benzyl radical mass spectrum.[53] Because of dissociative ionization, there is a daughter peak at m/z = 91 from the precursor molecule in the gray trace of Figure 2. However, once the m/z = 151 peak is

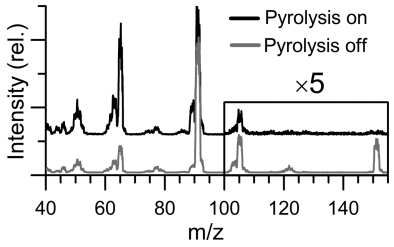

Figure 2. Mass spectrum of the molecular beam normalized to the m/z = 91 signal intensity with pyrolysis off (gray) and pyrolysis on (black). Upon heating the SiC tube, the peak at m/z = 151 disappears, and peaks at m/z = 90 and 65 increase in relative intensity.

depleted, as in the black trace of Figure 2, it is expected that the m/z = 91 peak comes solely from the benzyl radical.

Further confirmation of precursor depletion and benzyl formation was made possible by the installation of a new Extrel axial beam ionizer with the capability of low electron energy ionization. Ionization efficiency curves for m/z = 91 are shown in Figure 3 with pyrolysis off and on while keeping the emission

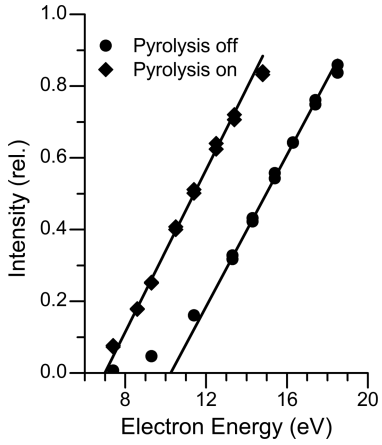

Figure 3. Ionization efficiency curves of m/z = 91 with pyrolysis off and on. The appearance potential for this signal with pyrolysis off is 10.2 eV, whereas with pyrolysis on, it is 7.0 eV.

current constant at 0.5 mA and normalized for signal intensity. The electron energy scale was calibrated by ionization of the noble gases He, Ne, Ar, and Kr. The appearance energy is the extrapolated intercept from the linear region of the curve. The appearance energy of m/z = 91 with pyrolysis off was determined to be 10.2 eV, which indicates it is due to dissociative ionization, while with pyrolysis on the appearance energy of 7.0 eV matches the expected ionization energy of 7.2 eV of the benzyl radical.[54]

The benzyl radical beam velocity was characterized with a spinning slotted chopper wheel. Typical beam velocities were around 1800 m/s with speed ratios, defined as the beam flow velocity divided by the velocity spread, in the range of 4−5.

III. ELECTRONIC STRUCTURE AND RRKM CALCULATIONS

RRKM calculations have been performed as a comparison to the experimental analysis. The stationary points of interest are depicted on the potential energy diagram in Figure 1 and are collected from refs 7, 8, 41, and 43. TS8 and TS10 were determined using variational transition state theory with a 0.2 Å step size. Geometries, vibrational frequencies, and the zero

DOI: 10.1021/acs.jpca.5b07125
J. Phys. Chem. A 2015, 119, 12349−12356

point energy at each step were calculated at the B3LYP/6-31+G(d,p) level using Gaussian 09,[55] and the energies were reevaluated using MOLPRO[56] at the CCSD(T)/CBS level from the cc-pVDZ and cc-pVTZ basis sets using the scaling suggested by Martin.[57] The energies of the stationary points that were not previously reported at this level of theory were reevaulated using the above method from their reported geometries. The transitional modes were all treated in the harmonic oscillator approximation. The lowest vibrational frequency for W3, W6, W12, TS9, TS10, and TS17 was below 100 cm^{-1} and was thus treated as a free internal rotor with each internal rotational constant calculated from the reported or calculated (TS10) geometry. The densities and sums of states for each local minimum and transition state were calculated using the Beyer−Swinehart algorithm[58] with the reported energies and vibrational frequencies treated as harmonic oscillator frequencies. Individual rate constants were calculated using the microcanonical RRKM equation. The maximum energy was given by the photon energy. No tunneling effects were considered. All reaction pathways shown in Figure 1 were considered, using the steady state approximation on intermediate local minima to solve for the relative rates for each channel.

IV. RESULTS

TOF spectra at m/z = 90, $C_7H_6^+$, were measured at laboratory scattering angles Θ_{Lab} = 4°, 5°, and 6° with respect to the molecular beam axis and are shown as open circles in Figure 4.

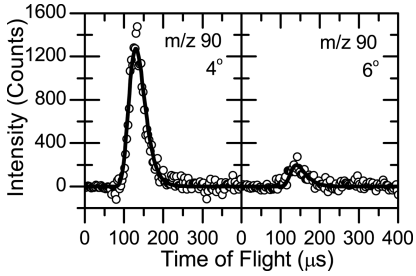

Figure 4. Representative TOF spectra of m/z = 90 at 4° and 6°. The open circles are data points, and the solid line is a simulation based on the $P(E_T)$ distribution in Figure 8.

TOF spectra at m/z = 76, $C_6H_4^+$, were detected at laboratory angles ranging from Θ_{Lab} = 4° up to 18°. Representative spectra are shown in Figure 5 (open circles). Additional TOF spectra were taken at the dissociative ionization masses of the above parent fragments at m/z = 74 and m/z = 50, shown in Figure 6;

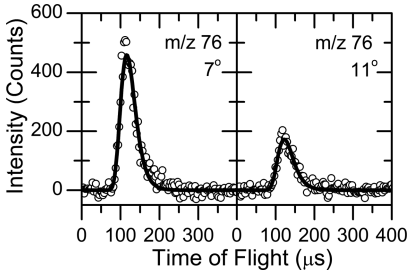

Figure 5. Representative TOF spectra of m/z = 76 at 7° and 11°. The open circles are data points, and the solid line is a simulation based on the $P(E_T)$ distribution in Figure 9.

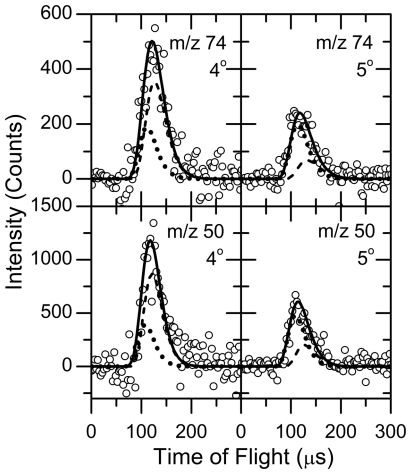

Figure 6. TOF spectra of m/z = 74 and 50 collected at 4° and 5°. The data are shown as open circles. The simulation has two components: the dashed line comes from the H loss $P(E_T)$ of Figure 8, and the dotted line comes from the CH_3 loss $P(E_T)$ of Figure 9. The solid line is the summed simulation.

these spectra are used to determine product branching ratios as discussed in section V. Signals at m/z = 26 and m/z = 65, the masses of the acetylene and cyclopentadienyl photoproduct parent ions, were extensively searched for but not observed.

Other sources of signal besides the benzyl radical photodissociation were assessed. We looked at the photodissociation of the precursor, 2-phenylethyl nitrite, with the pyrolysis source off and found one primary pathway that mimicked the pyrolysis reaction in Scheme 1, forming benzyl (m/z = 91), NO (m/z = 30), and formaldehyde (m/z = 30). With pyrolysis on, there was no longer any measured photodissociation signal at m/z = 91 or m/z = 30 off the beam axis, suggesting that precursor photodissociation is no longer present. The precursor reagent, 2-phenylethanol, also photodissociates to m/z = 91, so the lack of signal at m/z = 91 also eliminates it as a TOF contaminant. Bibenzyl may be formed in the SiC microreactor and may also photodissociate to form the stable benzyl radical; however, it too is eliminated by the absence of m/z = 91 signal away from the molecular beam. A contaminant at m/z = 105 ($C_8H_9^+$) is present in the molecular beam with the pyrolysis source on and the precursor parent m/z peak absent, as seen from the black trace in Figure 2. This feature may stem from C_8H_9 radicals formed in the SiC tube from the loss of ONO from the precursor molecule. Considering this formation scenario, the structure of this radical is likely either $C_6H_5CH_2C\bullet H_2$, 2-phenyleth-1-yl, or the more stable isomer, $C_6H_5C\bullet HCH_3$, 1-phenyleth-1-yl.[59] If such a radical was produced and photodissociated, we would expect to see an H atom loss channel forming the stable styrene molecule (m/z = 104),[59] but no photodissociation signal at any m/z > 90 is observed. It thus appears all signals in Figures 4−6 originate from benzyl radical photodissociation.

Possible contributions from two photon processes were assessed by conducting a laser power dependence study. TOF spectra taken at m/z = 90 and 85 mJ/cm^2 had a fast edge that did not depend linearly on laser power. At 50 mJ/cm^2 and below, the fast edge was reduced and the signal intensity had a linear dependence on laser power, in agreement with the laser power study done by Song et al.[40]

DOI: 10.1021/acs.jpca.5b07125
J. Phys. Chem. A 2015, 119, 12349−12356

V. ANALYSIS

Conservation of energy in this experiment is expressed by

$$E_{avail} = h\nu + E_0 - D_0 = E_{int} + E_T \quad (5)$$

The available energy (E_{avail}) to the photoproducts is the photon energy ($h\nu$) and any initial internal energy (E_0) minus the dissociation energy (D_0) for the specific channel. This available energy can either go into the internal energy of the products (E_{int}) or into their relative translational energy (E_T). The initial internal energy of the benzyl radical following supersonic jet expansion is unknown but is approximated as zero for purposes of analysis, supported by our previous work on phenyl radical expansions seeded in He with ~10% N_2.[51]

When all of the available energy is partitioned into translational energy, the maximum laboratory scattering angle can be calculated with knowledge of the benzyl beam velocity. On the basis of the most energetically favorable pathway for H loss in which fulvenallene is formed, channel 1, the m/z = 90 fragment should only be present up to a laboratory scattering angle of Θ_{Lab} = 6°. This restriction is depicted in the Newton diagram of Figure 7 and reflects the large mass ratio in the recoiling fragments, 90:1. The dashed circle represents the fastest possible center-of-mass velocities for the fulvenallene fragment. As no signal at m/z = 90 was observed beyond Θ_{Lab} = 6°, the Newton diagram supports the assignment of the m/z = 90 signal to the H loss channel from benzyl.

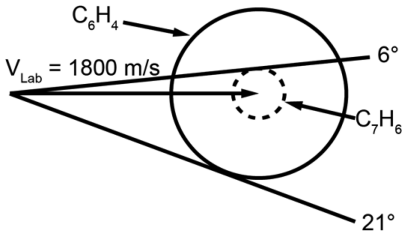

Figure 7. Newton diagram for benzyl photodissociation at 248 nm. Each circle represents the maximum center-of-mass velocities of the photofragment; the dashed circle denotes the C_7H_6 fragment, and the solid circle denotes the C_6H_4 fragment. The maximum scattering angles are shown.

Signal at m/z = 76 was present at laboratory angles well beyond where m/z = 90 was detected and therefore cannot be due to dissociative ionization of C_7H_6. The solid circle in Figure 7 represents the maximum center-of-mass velocities for the benzyne fragment and indicates that the m/z = 76 fragment should scatter up to a laboratory scattering angle of Θ_{Lab} = 21°. The angular distribution of the m/z = 76 fragment supports the assignment of this signal to CH_3 loss from benzyl, channel 3, as it was measured out to 18°. The m/z = 1 and m/z = 15 counterfragments for the two channels are kinematically allowed at all laboratory angles, which, combined with high detector background at these mass-to-charge values, prohibited their detection.

The photofragment TOF spectra are governed by the center-of-mass angular and translational energy distribution, $P(E_T,\theta)$. The total distribution can be uncoupled to yield

$$P(E_T,\theta) = P(E_T) \times I(\theta,E_T) \quad (6)$$

where $P(E_T)$ is the center-of-mass translational energy distribution and $I(\theta,E_T)$ is the center-of-mass angular distribution. The TOF spectra are analyzed using PHOTRAN,[60] a forward convolution program that simulates the TOF spectra given the center-of-mass angular and translational energy distributions. An initial guess of the $P(E_T)$ distribution is iteratively adjusted until good agreement is reached between the data and the simulation. The analysis assumes that the benzyl radical photodissociation is isotropic, which results in an adequate simulation of the present data. This assumption has been verified by Song et al.[40] for the H loss channel.

Characteristics of the $P(E_T)$ distributions are collected in Table 1. Figure 8 shows the $P(E_T)$ distribution for H loss; the resulting TOF simulations are shown as solid lines in Figure 4. The peak energy is 4 kcal/mol with an average translational energy, $\langle E_T \rangle$, of 7.1 kcal/mol and a maximum translational energy, E_{Tmax}, of 30 kcal/mol. The average fraction of energy that goes into translation, $\langle f_T \rangle$, is 0.2. The peak is very close to 0 kcal/mol and the average translational energy is much lower than the available energy, indicating that the photofragments have a large amount of internal excitation. The $P(E_T)$ extends up to 30 kcal/mol, which is close to the available energy of 35 kcal/mol if fulvenallene is the C_7H_6 fragment. The $P(E_T)$ distribution for H loss from benzyl photodissociation at 254 nm by Song et al.[40] has an average translational energy of 9.2 kcal/mol and is in excellent agreement with the distribution in Figure 8. Its characteristics are also shown in Table 1 for comparison.

Table 1. Characteristics of the $P(E_T)$ Distributions in Figures 8 and 9 and from Song et al. at 254 nm[a]

channel	peak (kcal/mol)	$\langle E_T \rangle$ (kcal/mol)	E_{Tmax} (kcal/mol)	E_{avail} (kcal/mol)	$\langle f_T \rangle$
H loss	4	7.1	30	35	0.2
H loss from Song et al.[a]	5.5	9.2	32.2	35	0.29
CH_3 loss	1	2.9	23	24	0.12

[a]Reference 40.

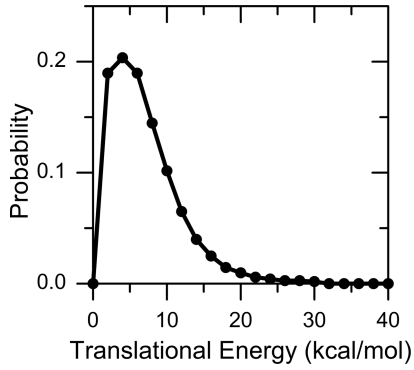

Figure 8. Center-of-mass $P(E_T)$ distribution for benzyl photodissociation to C_7H_6 + H. Details of the $P(E_T)$ distribution can be found in Table 1.

The $P(E_T)$ distribution for CH_3 loss is shown in Figure 9 with the resulting simulations of the m/z = 76 TOF spectra shown as solid lines in Figure 5. It is peaked at 1 kcal/mol with an average translational energy of 2.9 kcal/mol and an $\langle f_T \rangle$ of 0.12 and extends to a maximum energy of 23 kcal/mol, in agreement with the 24 kcal/mol available energy. The very weak high translational energy component of this distribution, shown in the inset of Figure 9, is necessary for agreement between the simulations and all TOF data. Since this $P(E_T)$ distribution was determined from TOF spectra obtained for

DOI: 10.1021/acs.jpca.5b07125
J. Phys. Chem. A 2015, 119, 12349−12356

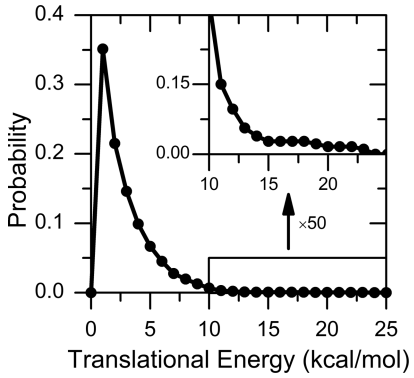

Figure 9. Center-of-mass $P(E_T)$ distribution for benzyl photodissociation to C_6H_4 + CH_3. Details of the $P(E_T)$ distribution can be found in Table 1.

$\Theta_{Lab} \geq 7°$, points in the $P(E_T)$ distribution below 2 kcal/mol are uncertain. This channel from benzyl photodissociation has not been reported before, and there is no $P(E_T)$ with which to compare.

Because of extensive dissociative ionization that occurs from electron impact ionization at 70 eV, there are m/z values that have components from both H loss and CH_3 loss products, and TOF spectra at these values are useful for estimating branching ratios for the two channels. Within the Newton circle for H loss, the photodissociation signal at m/z = 74 and m/z = 50 cannot be well simulated by either $P(E_T)$ alone; components from both channels are required for the spectra to be well-simulated. Figure 6 shows spectra at m/z = 74 and m/z = 50 with the total simulation in the solid line and components from each dissociation pathway as dashed and dotted lines.

The branching ratio (BR) between the two channels can be calculated using eq 7.

$$\mathrm{BR}\ (\mathrm{CH_3\ loss/H\ loss}) = \frac{W_{\mathrm{CH_3}}}{W_{\mathrm{H}}} \times \frac{\sigma_{\mathrm{H}}}{\sigma_{\mathrm{CH_3}}} \times \frac{f_{\mathrm{H}}}{f_{\mathrm{CH_3}}} \qquad (7)$$

The weighting of each $P(E_T)$, W_i, in the TOF simulation was determined by matching the total simulation to the data with consistent weighting at all angles. This weighting was then normalized by the ionization cross section, σ_i, of the parent fragment, estimated by the scheme of Fitch and Sauter,[61] and by f_i, the probability that each parent fragment will dissociatively ionize to m/z = 74 or m/z = 50. This probability was determined by collecting signal at Θ_{Lab} = 4° for all m/z values with measurable signal intensity (90, 89, 88, 87, 86, 85, 84, 76, 75, 74, 73, 64, 63, 62, 61, 60, 51, 50, 49, 39, 38) and then determining the fraction that appears at the specific m/z value of interest. All of the m/z values mentioned have a component from H loss, but the CH_3 + benzyne channel is only observed at m/z = 76 (40%), 74 (20%), 73 (6%), and 50 (34%) in qualitative agreement with the dominant m/z values observed with benzyne formed from phenyl photodissociation.[51] Taking all of these factors into account, the experimental branching ratio of CH_3/H loss is 0.011 ± 0.004. The uncertainty comes from the variation in branching ratio calculated from different angles (4° and 5°) and different masses (m/z = 74 and m/z = 50). This ratio indicates that H loss is the dominant pathway with only minor contributions from CH_3 loss.

VI. DISCUSSION

The goal of this study was to assess how the benzyl radical photodissociates after excitation at 248 nm in a collisionless environment with interest in identifying the photofragments and the dissociation mechanism. The results of this study suggest that there are two competing pathways, an H loss pathway and a methyl loss pathway.

The existence of an H loss channel from benzyl has been ascertained by shock tube studies, photodissociation studies, and thermolysis studies.[35,36,39,40,62,63] Although the other fragment measured in this experiment at m/z = 90 has not been unambiguously identified, theoretical work has suggested that it is most likely the fulvenallene molecule.[7,8,41,42] The identification of an H loss channel is corroborated here by the agreement between the Newton diagram in Figure 7 with the angular distribution of signal and by the excellent agreement between the $P(E_T)$ distribution from Song et al., based on measuring the H atom fragment, with our $P(E_T)$ in Figure 8, determined from TOF spectra for the C_7H_6 counterfragment. We cannot differentiate between the production of fulvenallene and 2-ethynylcyclopentadiene or distinguish which pathway in Figure 1 produces fulvenallene because all of these pathways are energetically very similar.

The methyl loss channel is relatively new to the benzyl dissociation landscape with little mention in the literature. The theoretically reported[7] energetics agree with the extent of the $P(E_T)$ distribution in Figure 9. In addition, the assignment of the m/z = 76 fragment as benzyne is corroborated by the qualitative agreement with the dissociative ionization pattern measured for this product from phenyl photodissociation.[51] Unfortunately, the corresponding methyl fragment was not detected, and thus, using conservation of momentum to match the partner fragments was not possible.

The shape of the $P(E_T)$ distributions in Figures 8 and 9 suggest that the dissociation mechanisms for both H loss and CH_3 loss involve internal conversion to the ground electronic state followed by energy randomization and dissociation. The maximum energy in both distributions agrees with the available energy calculated with ground state products. Time resolved photoionization studies determined an excited state lifetime of 150 fs for the $\tilde{D}^2B_2$ state following excitation at 255 nm and suggested a stepwise internal conversion to the $\tilde{A}/\tilde{B}$ states whose estimated lifetime of less than 2 ps returns the benzyl radical to the ground state.[49,64] Therefore, dissociation on an electronically excited state is unlikely. Both $P(E_T)$ distributions peak close to zero, which indicates a high degree of internal excitation consistent with energy randomization and dissociation from a bound potential.

If internal conversion to the ground state is followed by rapid intramolecular vibrational redistribution, then RRKM calculations would be a reasonable theoretical framework for experimental comparison. Considering all possible pathways from benzyl as depicted in Figure 1, the calculated branching ratio for CH_3/H loss (combined fulvenallene and 2-ethynylcyclopentadiene) is 0.027. Omitting any effects of tunneling reduces the rate of any reaction involving H motion; as these transitions are present for both the H loss pathways and the CH_3 loss pathway, the effect of including tunneling is unclear. Within the limitations of this analysis, the reported RRKM branching ratio indicates that H loss is the dominant dissociation channel, in good agreement with the experimental branching ratio of 0.011 ± 0.004. In addition, RRKM

DOI: 10.1021/acs.jpca.5b07125
J. Phys. Chem. A 2015, 119, 12349−12356

calculations showed that fulvenallene is the dominant H loss product over 2-ethynylcyclopentadiene with a branching ratio of 77:1. Furthermore, RRKM calculations for the formation of acetylene + cyclopentadienyl indicate that it is 6.7 times less likely to occur than the formation of methyl and benzyne and 250 times less likely than H loss from benzyl. A more complete RRKM study of the benzyl radical ground state dissociation would be of great interest.

Although channel 4, acetylene + cyclopentadienyl, has a lower asymptotic energy than either H atom or methyl loss, the pathway to its formation has more steps with higher and tighter barriers compared to the other channels.[43] Buckingham et al.[36] claimed to observe both of these species, although they may not be from collisionless primary benzyl dissociation. It is possible that a photon energy higher than 248 nm is necessary for this pathway to occur.

VII. CONCLUSION

Photodissociation of the benzyl radical was studied upon excitation at 248 nm. There is evidence that supports two dissociation channels: H + C_7H_6, with the C_7H_6 fragment likely to be fulvenallene, and CH_3 + benzyne. Both of these channels have been predicted theoretically, and all of the experimental analysis supports the identifications made above. Both dissociation channels are attributed to internal conversion to the ground state followed by intramolecular vibration energy redistribution and dissociation. This mechanism is supported by the shape of each $P(E_T)$ distribution and by the agreement between the experimental branching ratio of 0.011 ± 0.004 in favor of H atom loss with RRKM calculations.

AUTHOR INFORMATION

Corresponding Author

*E-mail: dneumark@berkeley.edu.

Notes

The authors declare no competing financial interest.

ACKNOWLEDGMENTS

The authors thank Prof. Carlo Cavallotti and Prof. Piergiorgio Casavecchia for helpful discussions. This work was supported by the Director, Office of Basic Energy Sciences, Chemical Sciences, Geosciences, and Biosciences division of the U.S. Department of Energy under Contract DE-AC02-05CH11231.

REFERENCES

(1) Davis, W. M.; Heck, S. M.; Pritchard, H. O. Theoretical study of benzyl radical reactivity in combustion systems. *J. Chem. Soc., Faraday Trans.* **1998**, *94* (18), 2725−2728.

(2) Sivaramakrishnan, R.; Tranter, R. S.; Brezinsky, K. High pressure pyrolysis of toluene. 2. modeling benzyl decomposition and formation of soot precursors. *J. Phys. Chem. A* **2006**, *110* (30), 9400−9404.

(3) Barfknecht, T. R. Toxicology of soot. *Prog. Energy Combust. Sci.* **1983**, *9* (3), 199−237.

(4) Colket, M. B.; Seery, D. J. Reaction mechanisms for toluene pyrolysis. *Symp. (Int.) Combust., [Proc.]* **1994**, *25* (1), 883−891.

(5) Detilleux, V.; Vandooren, J. Experimental and kinetic modeling evidences of a C_7H_6 pathway in a rich toluene flame. *J. Phys. Chem. A* **2009**, *113* (41), 10913−10922.

(6) Tian, Z.; Pitz, W. J.; Fournet, R.; Glaude, P.-A.; Battin-Leclerc, F. A detailed kinetic modeling study of toluene oxidation in a premixed laminar flame. *Proc. Combust. Inst.* **2011**, *33* (1), 233−241.

(7) Derudi, M.; Polino, D.; Cavallotti, C. Toluene and benzyl decomposition mechanisms: elementary reactions and kinetic simulations. *Phys. Chem. Chem. Phys.* **2011**, *13* (48), 21308−21318.

(8) Polino, D.; Parrinello, M. Combustion chemistry via metadynamics: benzyl decomposition revisited. *J. Phys. Chem. A* **2015**, *119* (6), 978−989.

(9) Schüler, H.; Reinebeck, L.; Koberle, R. Über das auftreten von gemeinsamen bruchstücken (mehratomige radikale?) bei benzolderivaten in der glimmentladung. *Z. Naturforsch., A: Phys. Sci.* **1952**, *7* (6), 421−427.

(10) Bayrakceken, F.; Nicholas, J. E. A flash photolytic study of the benzyl and alpha-chlorobenzyl radicals. *J. Chem. Soc. B* **1970**, No. 0, 691−694.

(11) Porter, G.; Savadatti, M. I. The electronic spectra of benzyl—a new transition. *Spectrochim. Acta, Part A* **1966**, *22* (5), 803−806.

(12) Jacox, M. E. Vibrational and electronic energy levels of polyatomic transient molecules. In *NIST Chemistry WebBook*; Linstom, P. J., Mallard, W. G., Eds.; NIST Standard Reference Database Number 69; NIST: Gaithersburg, MD.10.1063/1.1497629

(13) Okamura, T.; Charlton, T. R.; Thrush, B. A. Laser-induced fluorescence of benzyl radicals in the gas phase. *Chem. Phys. Lett.* **1982**, *88* (4), 369−371.

(14) Selco, J. I.; Carrick, P. G. Jet cooled emission spectra of toluene and the benzyl radical. *J. Mol. Spectrosc.* **1989**, *137* (1), 13−23.

(15) Fukushima, M.; Obi, K. Jet spectroscopy of benzyl and benzyl-α-d_2. *J. Chem. Phys.* **1992**, *96* (6), 4224−4232.

(16) Lin, T.-Y. D.; Tan, X.-Q.; Cerny, T. M.; Williamson, J. M.; Cullin, D. W.; Miller, T. A. High-resolution fluorescence excitation spectra of jet-cooled benzyl and p-methylbenzyl radicals. *Chem. Phys.* **1992**, *167* (1−2), 203−214.

(17) Eiden, G. C.; Weisshaar, J. C. Vibronic coupling mechanism in the $\tilde{A}^2A_2$−$\tilde{B}^2B_2$ excited states of benzyl radical. *J. Chem. Phys.* **1996**, *104* (22), 8896−8912.

(18) Tonokura, K.; Koshi, M. Cavity ring-down spectroscopy of the benzyl radical. *J. Phys. Chem. A* **2003**, *107* (22), 4457−4461.

(19) Cossart-Magos, C.; Leach, S. Determination of the symmetry of the first excited electronic state of benzyl by rotational contour analysis of vibronic bands of the emission spectra of $C_6H_5CH_2$, $C_6H_5CD_2$, and $C_6D_5CD_2$. *J. Chem. Phys.* **1972**, *56* (4), 1534−1545.

(20) Cossart-Magos, C.; Leach, S. Two-mode vibronic interaction between neighboring 1^2A_2 and 2^2B_2 excited electronic states of the benzyl radical. *J. Chem. Phys.* **1976**, *64* (10), 4006−4019.

(21) Orlandi, G.; Poggi, G.; Zerbetto, F. Vibronic coupling in the benzyl radical. *Chem. Phys. Lett.* **1985**, *115* (3), 253−258.

(22) Negri, F.; Orlandi, G.; Zerbetto, F.; Zgierski, M. Z. Quantum chemical and vibronic analysis of the $1^2B_2 \leftrightarrow 1^2A_2$, 2^2B_2 transition in benzyl-h_7 and benzyl-d_7 radicals. *J. Chem. Phys.* **1990**, *93* (1), 600−608.

(23) Boyd, A. A.; Noziere, B.; Lesclaux, R. Kinetics and thermochemistry of the reversible combination reactions of the allyl and benzyl radicals with NO. *J. Phys. Chem.* **1995**, *99* (27), 10815−10823.

(24) Matsugi, A.; Miyoshi, A. Kinetics of the self-reactions of benzyl and *o*-xylyl radicals studied by cavity ring-down spectroscopy. *Chem. Phys. Lett.* **2012**, *521* (0), 26−30.

(25) da Silva, G.; Bozzelli, J. W. Kinetic modeling of the benzyl + HO_2 reaction. *Proc. Combust. Inst.* **2009**, *32* (1), 287−294.

(26) da Silva, G.; Hamdan, M. R.; Bozzelli, J. W. Oxidation of the benzyl radical: mechanism, thermochemistry, and kinetics for the reactions of benzyl hydroperoxide. *J. Chem. Theory Comput.* **2009**, *5* (12), 3185−3194.

(27) Matsugi, A.; Miyoshi, A. Computational study on the recombination reaction between benzyl and propargyl radicals. *Int. J. Chem. Kinet.* **2012**, *44* (3), 206−218.

(28) Matsugi, A.; Miyoshi, A. Reactions of o-benzyne with propargyl and benzyl radicals: potential sources of polycyclic aromatic hydrocarbons in combustion. *Phys. Chem. Chem. Phys.* **2012**, *14* (27), 9722−9728.

(29) da Silva, G.; Bozzelli, J. W. Kinetics of the benzyl + $O(^3P)$ reaction: a quantum chemical/statistical reaction rate theory study. *Phys. Chem. Chem. Phys.* **2012**, *14* (46), 16143−16154.

DOI: 10.1021/acs.jpca.5b07125
J. Phys. Chem. A 2015, 119, 12349−12356

(30) Smith, R. D. A direct mass spectrometric study of the mechanism of toluene pyrolysis at high temperatures. *J. Phys. Chem.* **1979**, *83* (12), 1553−1563.
(31) Baulch, D. L.; Bowman, C. T.; Cobos, C. J.; Cox, R. A.; Just, T.; Kerr, J. A.; Pilling, M. J.; Stocker, D.; Troe, J.; Tsang, W.; et al. Evaluated kinetic data for combustion modeling: Supplement II. *J. Phys. Chem. Ref. Data* **2005**, *34* (3), 757−1397.
(32) Jones, J.; Bacskay, G. B.; Mackie, J. C. Decomposition of the benzyl radical: quantum chemical and experimental (shock tube) investigations of reaction pathways. *J. Phys. Chem. A* **1997**, *101* (38), 7105−7113.
(33) Oehlschlaeger, M. A.; Davidson, D. F.; Hanson, R. K. High-temperature thermal decomposition of benzyl radicals. *J. Phys. Chem. A* **2006**, *110* (21), 6649−6653.
(34) Sivaramakrishnan, R.; Su, M. C.; Michael, J. V. H- and D-atom formation from the pyrolysis of $C_6H_5CH_2Br$ and $C_6H_5CD_2Br$: Implications for high-temperature benzyl decomposition. *Proc. Combust. Inst.* **2011**, *33* (1), 243−250.
(35) Lemieux, J. M. Thermal decomposition of molecules relevant to combustion and chemical vapor deposition by flash pyrolysis time of flight mass spectrometry. Ph.D. Dissertation, University of California, Riverside, Riverside, CA, 2013.
(36) Buckingham, G. T.; Ormond, T. K.; Porterfield, J. P.; Hemberger, P.; Kostko, O.; Ahmed, M.; Robichaud, D. J.; Nimlos, M. R.; Daily, J. W.; Ellison, G. B. The thermal decomposition of the benzyl radical in a heated micro-reactor. I. Experimental findings. *J. Chem. Phys.* **2015**, *142* (4), 044307.
(37) Damm, M.; Deckert, F.; Hippler, H. Collisional deactivation of vibrationally highly excited benzyl radicals. *Ber. Bunsen-Ges. Phys. Chem.* **1997**, *101* (12), 1901−1908.
(38) Damm, M.; Deckert, F.; Hippler, H.; Rink, G. Specific rate constants for the fragmentation of vibrationally excited benzyl radicals. *Phys. Chem. Chem. Phys.* **1999**, *1* (1), 81−90.
(39) Fröchtenicht, R.; Hippler, H.; Troe, J.; Toennies, J. P. Photon-induced unimolecular decay of the benzyl radical: first direct identification of the reaction pathway to C_7H_6. *J. Photochem. Photobiol., A* **1994**, *80* (1−3), 33−37.
(40) Song, Y.; Zheng, X.; Lucas, M.; Zhang, J. Ultraviolet photodissociation dynamics of the benzyl radical. *Phys. Chem. Chem. Phys.* **2011**, *13* (18), 8296−8305.
(41) da Silva, G.; Cole, J. A.; Bozzelli, J. W. Thermal decomposition of the benzyl radical to fulvenallene (C_7H_6) + H. *J. Phys. Chem. A* **2009**, *113* (21), 6111−6120.
(42) Cavallotti, C.; Derudi, M.; Rota, R. On the mechanism of decomposition of the benzyl radical. *Proc. Combust. Inst.* **2009**, *32* (1), 115−121.
(43) da Silva, G.; Cole, J. A.; Bozzelli, J. W. Kinetics of the cyclopentadienyl + acetylene, fulvenallene + H, and 1-ethynylcyclopentadiene + H reactions. *J. Phys. Chem. A* **2010**, *114* (6), 2275−2283.
(44) Butler, L. J.; Neumark, D. M. Photodissociation dynamics. *J. Phys. Chem.* **1996**, *100* (31), 12801−12816.
(45) Lee, Y. T.; McDonald, J. D.; LeBreton, P. R.; Herschbach, D. R. Molecular beam reactive scattering apparatus with electron bombardment detector. *Rev. Sci. Instrum.* **1969**, *40* (11), 1402−1408.
(46) Negru, B.; Goncher, S. J.; Brunsvold, A. L.; Just, G. M. P.; Park, D.; Neumark, D. M. Photodissociation dynamics of the phenyl radical via photofragment translational spectroscopy. *J. Chem. Phys.* **2010**, *133* (7), 074302.
(47) Negru, B.; Just, G. M. P.; Park, D.; Neumark, D. M. Photodissociation dynamics of the *tert*-butyl radical via photofragment translational spectroscopy at 248 nm. *Phys. Chem. Chem. Phys.* **2011**, *13* (18), 8180−8185.
(48) Kohn, D. W.; Clauberg, H.; Chen, P. Flash pyrolysis nozzle for generation of radicals in a supersonic jet expansion. *Rev. Sci. Instrum.* **1992**, *63* (8), 4003−4005.
(49) Margraf, M.; Noller, B.; Schröter, C.; Schultz, T.; Fischer, I. Time- and frequency-resolved photoionization of the C^2A_2 state of the benzyl radical, C_7H_7. *J. Chem. Phys.* **2010**, *133* (7), 074304.
(50) Noyes, W. A. *Organic Syntheses*; Wiley & Sons: New York, 1943; Vol. *II*, p 108.
(51) Cole-Filipiak, N. C.; Shapero, M.; Negru, B.; Neumark, D. M. Revisiting the photodissociation dynamics of the phenyl radical. *J. Chem. Phys.* **2014**, *141* (10), 104307.
(52) Daly, N. R. Scintillation type mass spectrometer ion detector. *Rev. Sci. Instrum.* **1960**, *31* (3), 264−267.
(53) Pottie, R. F.; Lossing, F. P. Free radicals by mass spectrometry. XXIII. mass spectra of benzyl and α-d_2-benzyl free radicals. *J. Am. Chem. Soc.* **1961**, *83* (12), 2634−2636.
(54) Eiden, G. C.; Weisshaar, J. C. Adiabatic ionization potential of benzyl radical by two-color resonant two-photon ionization. *J. Phys. Chem.* **1991**, *95* (16), 6194−6197.
(55) Frisch, M. J.; Trucks, G. W.; Schlegel, H. B.; Scuseria, G. E.; Robb, M. A.; Cheeseman, J. R.; Scalmani, G.; Barone, V.; Mennucci, B.; Petersson, G. A.; et al. *Gaussian 09*; Gaussian, Inc.: Wallingford, CT, USA, 2009.
(56) Werner, H.-J.; Knowles, P. J.; Knizia, G.; Manby, F. R.; Schütz, M.; Celani, P.; Korona, T.; Lindh, R.; Mitrushenkov, A.; Rauhut, G.; et al. *MOLPRO*, version 2008.1, a package of ab initio program.
(57) Martin, J. M. L. Ab initio total atomization energies of small molecules — towards the basis set limit. *Chem. Phys. Lett.* **1996**, *259* (5−6), 669−678.
(58) Beyer, T.; Swinehart, D. F. Algorithm 448: number of multiply-restricted partitions. *Commun. ACM* **1973**, *16* (6), 379.
(59) *CRC Handbook of Chemistry and Physics*, 96th ed.; Haynes, W. M., Ed.; CRC Press: Boca Raton, FL, 2015.
(60) Harich, S. A. PHOTRAN, a program for forward convolution analysis of photodissociation, 2003.
(61) Fitch, W. L.; Sauter, A. D. Calculation of relative electron impact total ionization cross sections for organic molecules. *Anal. Chem.* **1983**, *55* (6), 832−835.
(62) Braun-Unkhoff, M.; Frank, P.; Just, T. High temperature reactions of benzyl radicals. *Ber. Bunsen-Ges. Phys. Chem.* **1990**, *94* (11), 1417−1425.
(63) Rao, V. S.; Skinner, G. B. Formation of hydrogen atoms in pyrolysis of ethylbenzene behind shock waves. Rate constants for the thermal dissociation of the benzyl radical. *Symp. (Int.) Combust., [Proc.]* **1988**, *21* (1), 809−814.
(64) Zierhut, M.; Noller, B.; Schultz, T.; Fischer, I. Excited-state decay of hydrocarbon radicals, investigated by femtosecond time-resolved photoionization: ethyl, propargyl, and benzyl. *J. Chem. Phys.* **2005**, *122* (9), 094302.

DOI: 10.1021/acs.jpca.5b07125
J. Phys. Chem. A 2015, 119, 12349−12356